electronics

MDPI

Article

A Buck-Boost Transformerless DC–DC Converter Based on IGBT Modules for Fast Charge of Electric Vehicles

Borislav Dimitrov [1,*], Khaled Hayatleh [1], Steve Barker [1], Gordana Collier [1], Suleiman Sharkh [2] and Andrew Cruden [2]

[1] School of Engineering, Computing and Mathematics, Oxford Brookes University, Wheatley campus, Oxford OX33 1HX, UK; khayatleh@brookes.ac.uk (K.H.); stevebarker@brookes.ac.uk (S.B.); gordanacollier@brookes.ac.uk (G.C.)

[2] Faculty of Engineering and the Environment, University of Southampton, University Road, Southampton SO17 1BJ, UK; S.M.Sharkh@soton.ac.uk (S.S.); A.J.Cruden@soton.ac.uk (A.C.)

* Correspondence: bdimitrov@brookes.ac.uk; Tel.: +44-(0)1865-482962

Received: 9 January 2020; Accepted: 25 February 2020; Published: 28 February 2020

Abstract: A transformer-less Buck-Boost direct current–direct current (DC–DC) converter in use for the fast charge of electric vehicles, based on powerful high-voltage isolated gate bipolar transistor (IGBT) modules is analyzed, designed and experimentally verified. The main advantages of this topology are: simple structure on the converter's power stage; a wide range of the output voltage, capable of supporting contemporary vehicles' on-board battery packs; efficiency; and power density accepted to be high enough for such a class of hard-switched converters. A precise estimation of the loss, dissipated in the converter's basic modes of operation Buck, Boost, and Buck-Boost is presented. The analysis shows an approach of loss minimization, based on switching frequency reduction during the Buck-Boost operation mode. Such a technique guarantees stable thermal characteristics during the entire operation, i.e., battery charge cycle. As the Buck-Boost mode takes place when Buck and Boost modes cannot support the output voltage, operating as a combination of them, it can be considered as critically dependent on the characteristics of the semiconductors. With this, the necessary duty cycle and voltage range, determined with respect to the input-output voltages and power losses, require an additional study to be conducted. Additionally, the tolerance of the applied switching frequencies for the most versatile silicon-based powerful IGBT modules is analyzed and experimentally verified. Finally, several important characteristics, such as transients during switch-on and switch-off, IGBTs' voltage tails, critical duty cycles, etc., are depicted experimentally with oscillograms, obtained by an experimental model.

Keywords: Buck-Boost; DC–DC; converter; fast battery charger; electric vehicles

1. Introduction

The technology of fast charge is an inevitable part of a future transport system based on electric vehicles, and has been proven by numerous studies [1–4]. Fast can be considered a charge cycle of 20 min to 40 min., during which the vehicle battery reaches 80% of its capacity. For this purpose, a significant amount of energy must be transferred from the source, which can be the electrical grid or stand-alone renewable energy source, etc. to the car battery. The equipment necessary for that purpose is a powerful electronic converter working as a battery charger.

Nowadays, the leading fast-charger schematics are based on different advanced switched-mode power supply topologies: LLC resonant converters with soft switching [5,6], phase-shift converters [7], two and three-level, three-phase, full-bridge direct current–direct current (DC–DC) converters [8,9],

bi-directional vehicle-to-grid converters [10], etc. These are advanced switch-mode converters which have significant technical advantages and, respectively, considerable areas of application. Their disadvantages are complexity, a high number of switches, high switching frequencies and therefore EMI (electromagnetic interference) problems, a complex control system, high price, difficulties with manufacturability, etc. Such problems can be avoided with a simple Buck-Boost structure based on isolated gate bipolar transistor (IGBT) modules.

The aim of this research is a powerful Buck-Boost transformerless converter, based on a small number of IGBT modules to be analyzed and experimentally verified. Such a solution has the potential to be used as a powerful (150 kW) battery charging system based on a budget-friendly topology with high power density and efficiency. These requirements are feasible due to the simple structure, which this type of DC–DC converter usually has. Inherently, their power stages are based on a small number of semiconductors. In this case, an application of the currently available powerful silicon-based IGBTs would allow for only two modules to be used.

Figure 1 shows the power part of transformerless fast-chargers based on Buck topology which is widely used today. Such charging stations are powered by a high-voltage distribution system through a low-frequency power transformer in order for their impact over the low-voltage system to be minimized. As a rectifier is usually used, a controllable alternating current – direct current (AC–DC) converter with PFC (power factor correction) is required. The analyzed and experimentally verified Buck-Boost converter based on powerful IGBT modules is designed to replace the Buck converters, as Figure 1 shows. The major benefit of a Buck-Boost converter topology is the inherent ability of the output voltage to be lower or bigger than the input DC voltage. Such a characteristic would guarantee the flexibility of the charging system and its applications in the wide range of growing battery-pack voltages.

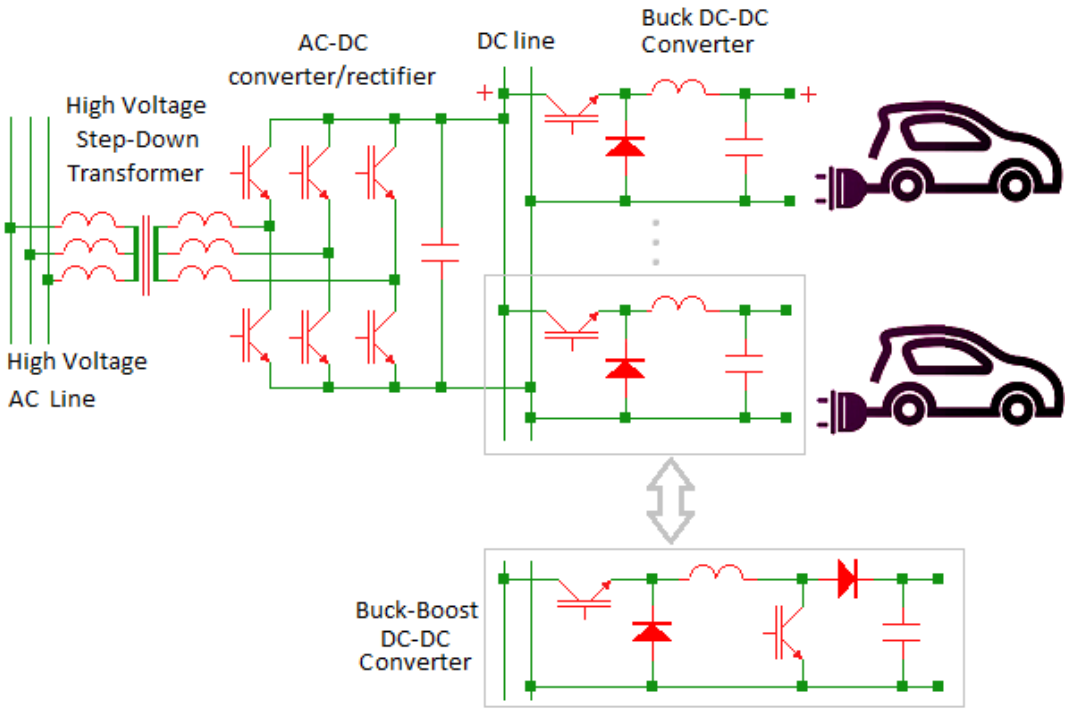

Figure 1. A fast-charge station with the main elements of direct current–direct current (DC–DC) Buck converters, low-frequency transformer; alternating current (AC)–DC converter-rectifier with power factor correction (PFC) and filter. The designed Buck-Boost converter is shown as a suggestion to replace the Buck converters.

The safe operation area (SOA), as one of the most important features, strongly depends on switching and conducting losses in a switch-mode application and, respectively the accumulated junction temperature. In [11] a study dedicated to over-current and over-temperature breakdown for high-voltage, high-current IGBT modules is presented. It is shown through simulations and experimental verification that breakdowns can happen when the modules operate in restrictive temperature environments. Although the paper is focused mainly on railway inverters, the presented analysis is supposed to be actual for DC–DC Buck-Boost converters as well. The same research gives information, according to which the maximum overloading, therefore the probable failure, occurs mostly when high current and high voltage are simultaneously applied across the device during the switch-on or switch-off periods. Additionally, the dependency of IGBTs dynamic characteristic on the temperature can be verified with modeling and simulations [12–14]. The proposed models have applications in converter design, mode-of-operation analysis, lifespan estimation, analysis and design of the necessary cooling system, etc.

A study of fast-charging under extreme temperature conditions is presented in [15]. This paper presents power-quality performance, addressing important characteristics such as ambient temperature range and its influence over the total harmonic distortion (THD), power factor, etc. Although this research is not focused on such issues, the concluded temperature range (+40 °C– −15 °C) and the considerations given for low THD are taken into account in this analysis.

Thermal modes of operation of IGBT modules are shown with modeling and simulation in [16,17]. The presented numerical analysis gives fundamental information about temperature dissipation and thermal field distribution in the modules. As the results are not focused on a specific converter, but rather a broader study is offered, they are applicable for a Buck-Boost converter in Buck, Boost and Buck-Boost modes of operation.

Two different IGBT structures, Floating Island (FLI) and Revers Conducting (RC-IGBT), are analyzed in [18] and [19,20] respectively. These technologies offer significant advantages such as a lower break-down voltage, which leads to lower losses and better efficiency, better robustness under fault conditions, etc. In [20] an application in high voltage railway converters is presented. A significant decrease in losses, accomplished with RC-IGBT modules compared to conventional IGBT modules, is shown. Such efficiency improvements can also be expected to be achieved for battery-charge applications based on the proposed topology, although the published literature in this direction is insufficient.

Potentially, Buck-Boost DC–DC transformerless converters can face short-circuit failure modes under certain conditions. Sources [21–26] offer significant information in this direction as follows: IGBT structural behavior under short-circuit [21]; breakdown and thermal runaway mechanisms leading to destructive failure [22]; damages from electrostatic discharge [23]; IGBTs' mechanical stress under short-circuit conditions [24]; turn-off failure mechanism [25]; robustness of IGBT modules during turn-off commutation.

In [25] experimentally obtained oscillograms are given, which clearly show the mechanism of turn-off failure of an IGBT module. The depicted problem with overcurrent leading to a thermal runway and avalanche breakdown is supposed to be actual for DC–DC Buck-Boost converters, especially on the border between Buck and Boost modes of operation. The same suggestions can be confirmed from the experimental data presented in [26].

The research showed that the Buck-Boost topology is used for low-voltage converters, based on MOSFETs (Metal Oxide Semiconductor Field Effect Transistor), completed by four transistors with synchronous switching [27–37]. Despite that, its application with high-voltage IGBTs, considering the different voltage ranges and transistors' parameters, requires the analysis and design procedure to be altered. The proposed application requires study to be undertaken in several directions: a possible range of the switching frequencies at the Buck-Boost mode of operation for a converter based on high-voltage and high-current IGBT modules; thermal mode of operation and possibilities for the dissipated losses and temperature, to be reduced; the possible voltage ranges between the three modes

of operation Buck, Boost and Buck-Boost to be analyzed and experimentally verified. Additionally, the low-voltage MOSFET converters are implemented with control systems based on application-specific integrated circuits (ASICs), directly powered by the low input voltage [38–41] usually in a range 24–60 V, which is inapplicable for high-voltage IGBT applications up to 1000 V. In this sense, the novelty in the current research consists in the application of high-voltage, high-power IGBT modules, half-bridge or integrated transistor-diode structures, applied for vehicles fast charge converters, which cannot be completed with the presented low-voltage applications. Such a technology needs further development in two directions.

The suggested Buck-Boost converter maintains three modes of operation: Buck, Boost, and Buck-Boost. The third applies on the border between Buck and Boost, as in this condition neither of them can support the output voltage. In [27–29] it is correctly suggested that the implementation of Buck-Boost mode has the potential to decrease the losses and to increase the efficiency of the DC–DC power stage. For this class of hard-switched converters, the targeted efficiency can be set at 97–98% for both semiconductors. In the currently available literature, the IGBT operation at Buck-Boost operation mode is not presented in detail, considering the relatively low switching frequency (8–16 kHz), significant voltage tails for the silicon-based IGBTs, and the necessary time rages.

The voltage region of the Buck-Boost operation mode is of primary importance for achieving a robust and efficient operation [35–37]. Several techniques are applicable mainly used for MOSFET-based DC–DC converters: active inductor balancing for interleaving Buck-Boost converters [35], reduction of the passive elements [36], and a high level of implementation of a digital control system for low power portable electronics. It depends on the semiconductors' parameters, or in this case, currents and voltage tails of the selected IGBT modules, the maximum duty cycle at Buck and Boost modes, and switching frequency, etc. Its importance requires it to be analyzed and verified experimentally.

The paper is organized as follows: section two presents an analysis of the proposed converter, which is limited to the power stage of the Buck and Boost parts; section three shows an experimental study, conducted with an experimental model; conclusions are summarized in section four.

2. Analysis of the Proposed Converter

Figure 2 shows the proposed Buck-Boost converter for fast battery charge, derived from the basic circuit, shown in Figure 1. The input power supply consists of a low-frequency three-phase isolation transformer Tr1, connected to low-voltage grid (0.4 kV), as in this case a high-voltage system has not been available. The voltage after rectification and filtering is 660 V, assumed to be stable on the input side of the DC–DC converter. As this part of the circuit is not the object of this research it has been simplified for experimental purposes only.

The Buck-Boost converter consists of two IGBT modules, M1 and M2, with transistor-diode structure Q1-D1 and Q2-D2, inductor L1, input C1 and output C2 capacitors, and snubber capacitors C3 and C4. The output voltage can vary in the range of 300–1000 V, depending on the vehicle battery (B1) type and state of charge (SoC). The transistor-diode modules, shown in Figure 2, are particularly designed for such type converters.

The transistor-diode modules, shown in Figure 2, are particularly designed for such a type of converter. Alternatively, half-bridge modules (Figure 3) can be used. Although additional control signals are necessary for transistors Q2 and Q3, for most of the modules only their reverse diodes can be used for simplification. Table A1 (Appendix A) shows some currently available IGBT modules, rated at the required power, offered by several manufacturers.

As mentioned above, a typical feature of these type of converters are the three modes of operation. First, the Buck mode when $V_{out} < V_{in}$, or in this analysis, a range 300–600 V is assumed (Figure 4). During Buck mode, the transistor Q1 is controlled by pulse width modulation (PWM) and transistor Q2 is permanently OFF. Module M1 dissipates switching and conductive losses, while only the diode from M2 has conductive losses.

The Boost operation mode is applicable when $V_{out} > V_{in}$, or here a range 700–1000 V. V_{out} is assumed. During Boost mode, the transistor Q2 is under PWM control and transistor Q1 is permanently ON. It is vice versa on the previous mode, M2 dissipates switching and conductive losses, while M1 only has conductive losses. Diode D1, module M1, is permanently OFF and can be accepted as excluded from the analysis.

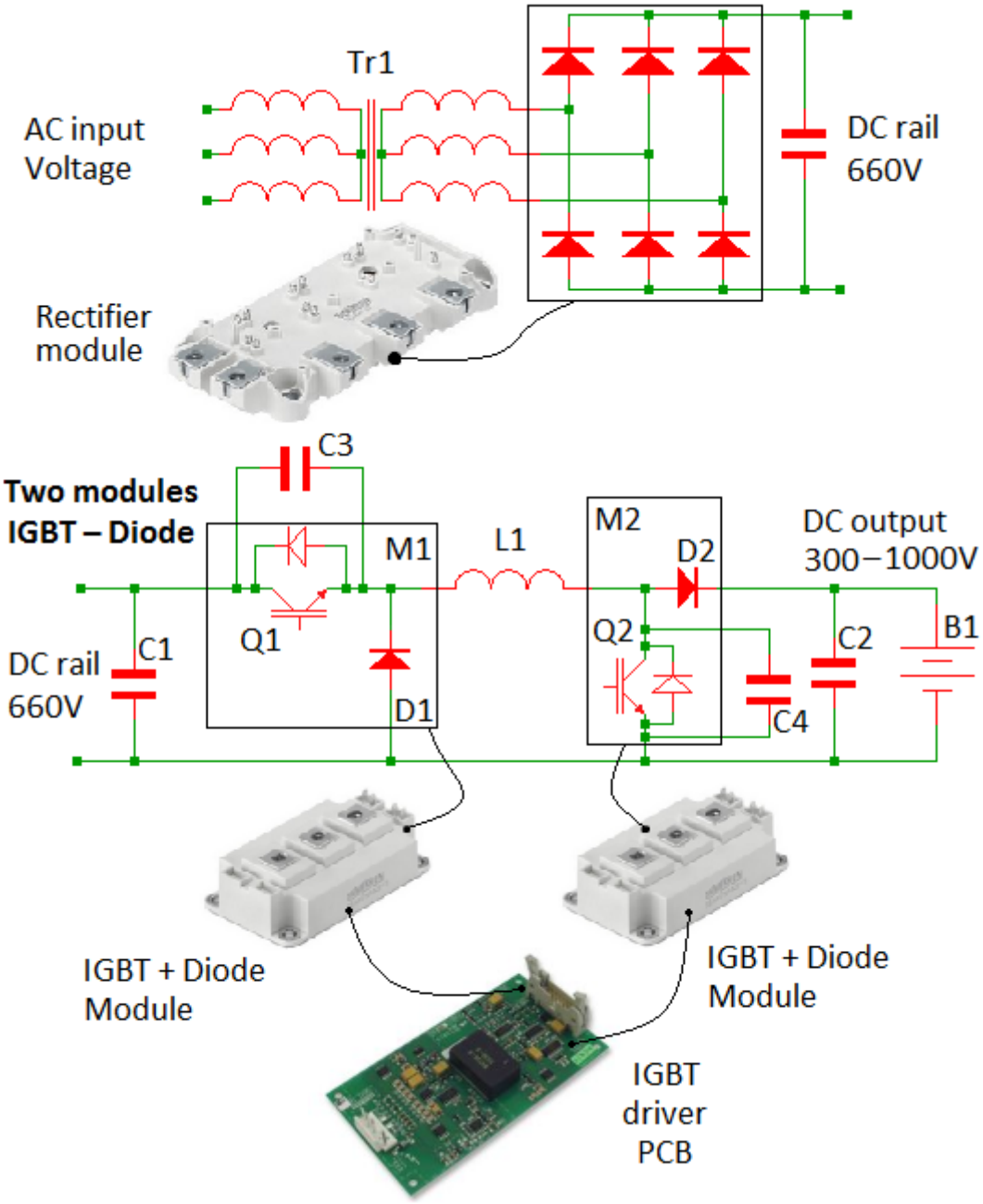

Figure 2. The proposed Buck-Boost converter for fast charge, based on isolated gate bipolar transistor (IGBT) modules (see Table A1 Appendix A).

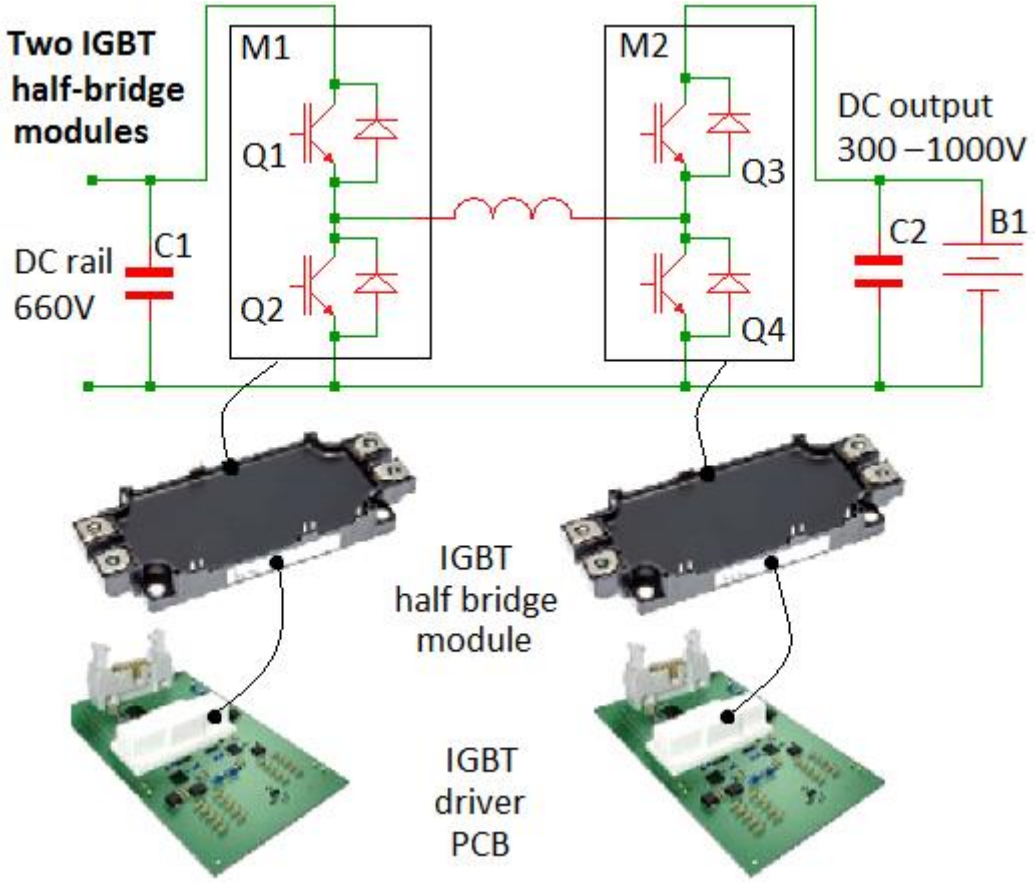

Figure 3. Buck-Boost converter, based on half-bridge IGBT modules with drivers (see Table A1 Appendix A).

The Buck-Boost mode is necessary when V_{out} and V_{in} are approximately equal and neither of previous modes can support the normal operation. The problem occurs due to the duty cycle, which under equalization between V_{out} and V_{in} will be too high during Buck mode or too low during the Boost mode of operation. Here, considering the input DC voltage of 660 V, a flexible range of $V_{out} > 550 - 600$ V and $V_{out} < 700 - 750$ V is assumed, as Figure 4 shows. In this mode IGBT module M1 operates as a Buck converter with a fixed duty cycle, between 0.7–0.8 and IGBT module M2 operates as a Boost converter with variable duty cycle 0.1–0.4 (Figure 5). The presented PWM signals are produced by a flexible control system based on microcontroller, current and voltage measurement of galvanically isolated circuits, shown in the same figure. These ranges are considered from manufacturers' documentation [38–41], where they are recommended only for MOSFET-based converters and should be checked for IGBTs. Another factor, which has a significant impact on the duty cycle restriction, is imposed from the snubber capacitors C3 and C4, Figure 2. As for the IGBT modules, due to their relatively low switched frequency and high voltages, they can reach 1.5–2 μF, i.e., much bigger than MOSFET-based applications, and therefore their effect over the operation modes must be verified experimentally.

Under the suggested sequence of modulation Buck, Buck-Boost and Boost, a smooth output voltage must be assured during the entire charging cycle, regardless of its stage-constant current or constant voltage. Eventually, the output current given in Figure 5 shows that the Buck, Boost, and Buck-Boost are continuous modes of operation.

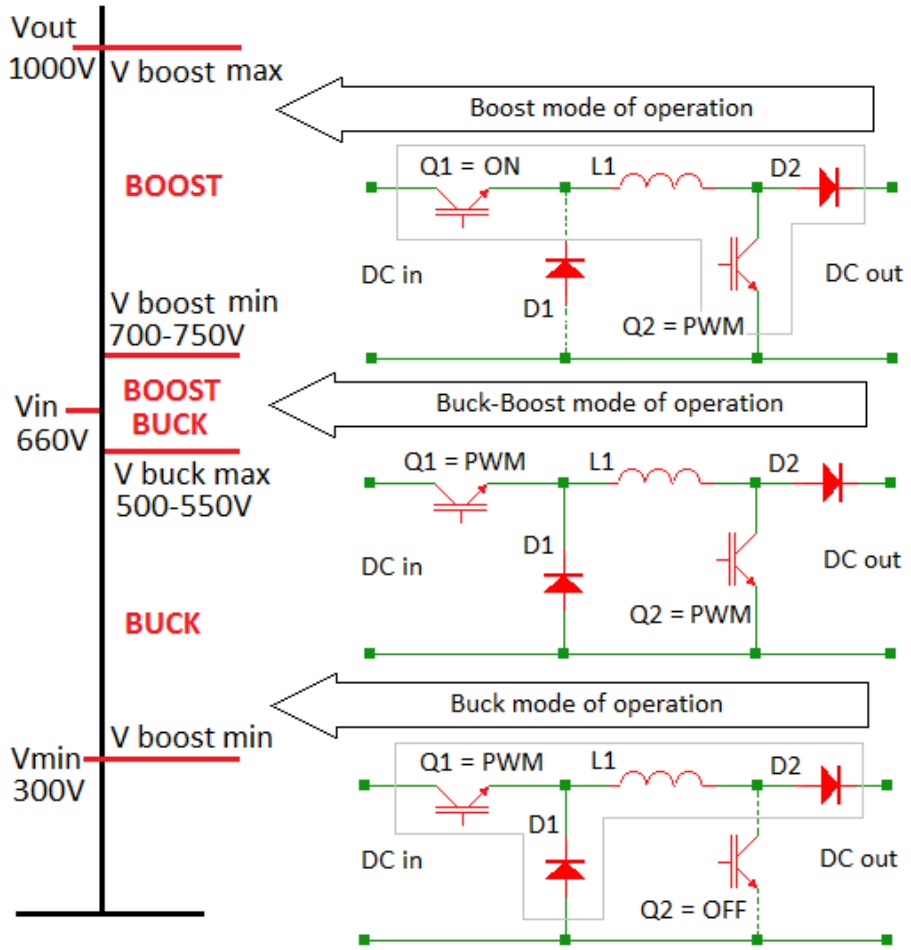

Figure 4. Buck, Boost and Buck-Boost modes of operations. Their activation and the necessary pulse width modulation (PWM) is presented according to the output voltage range.

D is the duty cycle; V_{out} is the output voltage; V_{in} is the input voltage; T is the period (sec); t_{on} is the ON time (sec); F_{sw} is the switching frequency (Hz); L is the inductance (H); $I_{\max out}$ is the maximum output current.

During Buck-Boost mode, modules M1 and M2 operate with PWM at the same time, dissipating switching and conductive losses. Such an operation has the potential to heat the converter to a dangerous temperature level, i.e., the problem presented above. Improving the cooling system is not always a universal solution, because it would have a negative impact on power density and overall efficiency [39,40]. Hence, other techniques for minimizing the losses must be implemented. The suggested approach in this research is the switching frequency to be reduced during Buck-Boost mode, and the necessary parameters of such reduction must be analyzed and verified [41].

As Buck and Boost mode of operations have trivial descriptions [42,43], although fundamental for this converter, their basic equations are given in Table 1 without further explanation.

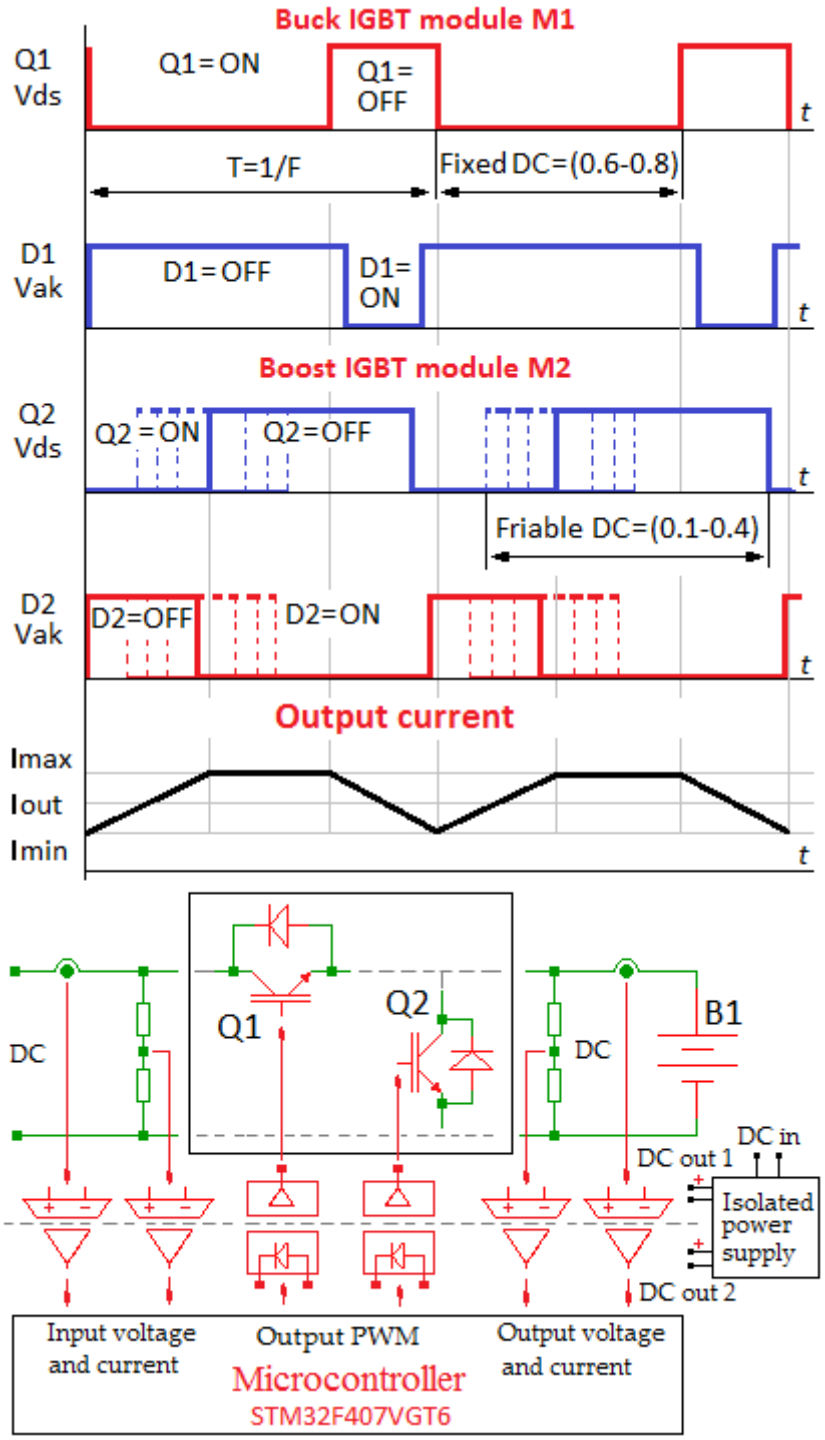

Figure 5. Buck-Boost mode of operation and block diagram of the control system.

Table 1. Buck and Boost mode of operations.

Buck	Boost
Duty Cycle	
$D_{Buck} = \frac{V_{out}}{V_{in}} = \frac{t_{on}}{T}$	$D_{Boost} = 1 - \frac{V_{in(min)}}{V_{out}}$
Inductor	
$L_{Buck} = \frac{V_{out}(1-D)}{F_{sw} \times \Delta I_L}$	$L_{Boost} = \frac{V_{IN(min)} \times D_{boost}}{F_{sw} \times \Delta I_L}$
Maximum output current	
$I_{\max out\ Buck} = I_L - \frac{\Delta I_L}{2}$	$I_{\max out\ Boost} = \left(I_{L(min)} \frac{\Delta I_L}{2}\right) \times (1 - D)$
Maximum switching current	
$I_{sw\max Buck} = \frac{\Delta I_{max}}{2} + I_{out}$	$I_{sw\max Boost} = \frac{\Delta I_{max}}{2} + \frac{I_{out}}{1-D_{boost}}$

The Buck-Boost mode of operation can be derived from Buck and Boost modes, as in this mode, both operations are cascaded. If the voltage after the Buck part of the converter is derived from buck duty cycle as [38]:

$$V_{out\ buck} = D_{buck} \times V_{in}, \tag{1}$$

and the output voltage, i.e., after the Boost part, is based on Boost duty cycle (2) as:

$$V_{out} = D_{boost} \times V_{out\ boost}, \tag{2}$$

then the Buck-Boost mode of operation can be written as:

$$\frac{V_{out}}{V_{in}} = D_{buck} \times D_{boost}, \tag{3}$$

leading to [38]:

$$\frac{V_{out}}{V_{in}} = \frac{D_{buck}}{1 - D_{boost}}, \tag{4}$$

The losses estimation is based on the following requirements: the converter must be designed to work with constant output current and constant output voltage. The voltage range is shown in Figure 3 as $V_{out.min} = 300$ V, $V_{out.max} = 1000$ V. The accepted current range for this design is $I_{out.nom} = 150$ A, $I_{out.peak} = 200$ A. With that, the converter must be able to work appropriately, i.e., on the required efficiency and thermal equilibrium, under the nominal output power of $P_{out.nom} = 150$ kW and peak power of $P_{out.peak} = 200$ kW.

Usually, the targeted efficiency for this class of transformerless, hard-switched converters is within the range 96–97%, and should not be smaller than 95% at any modes of operation. In this paper, the efficiency is estimated only for both modules M1 and M2 (Figure 2), as they are the major focus of this research. This means that the efficiency should be over 98% at the nominal current of 150 A, and over 97% at maximum current of 200 A, which gives enough energy budget for the final efficiency target of the entire converter to be achieved.

The nominal switching frequency is 12 kHz for the Buck and Boost operation modes but it can be reduced to 10 kHz in order for the expected losses under Buck-Boost mode to be minimized. The output voltage ripples should be no bigger than 20% in any mode of operation. Although some of the analyzed modules given in Table A1 (Appendix A) are rated at higher than 20 kHz frequencies, which has the potential to reduce the size of the inductor and output capacitors, this research has found that such switching frequencies are not feasible at the required power level for hard-switching topology.

The energy analysis is based on fundamental equations and dependencies for IGBT transistors, presented in the literature sources [44–48]. Because of that, in this case, the necessary mathematical apparat is simplified to the usage of basic equations for losses calculation and IGBT characteristics from manufacturers' datasheets [49–53].

The total losses of an IGBT are given as a sum of two components-conduction P_{cond} and switching P_{sw} losses, given by the Equation [46–48]:

$$P_{loss\ IGBT} = P_{cond} + P_{sw}, \tag{5}$$

As the switching losses are sum of turn ON and turn OFF losses, or

$$P_{sw} = P_{turn\ ON} + P_{trun\ OFF}, \tag{6}$$

can be written:

$$P_{loss\ IGBT} = P_{cond} + P_{turn\ ON} + P_{turn\ OFF}, \tag{7}$$

The conductive losses are calculated according to the current and the semiconductor resistance R_{on}, or:

$$P_{cond} = I_{RMS}^2 \times R_{on}, \tag{8}$$

The switching losses are calculated from the accumulated energies during the transient switched ON E_{ON}, switched OFF E_{off}, reverse recovery E_{rr}, and switched frequency f_{sw}, given from the equation [46–48]:

$$P_{sw} = \left(E_{ON} + E_{off} + E_{rr}\right) \times f_{sw}, \tag{9}$$

The necessary E_{ON}, E_{off}, E_{rr} can be obtained as functional current dependencies at given gate drive resistance, as shown in Figure 6 as an example. As for the suggested battery charger, the output current must vary in the wide area $I_{min} = 100\text{A} - I_{nom} = 150\text{A} - I_{max} = 200$ A, the necessary energies are in a range of several tents mJ, shown in the dashed area in the same pictures.

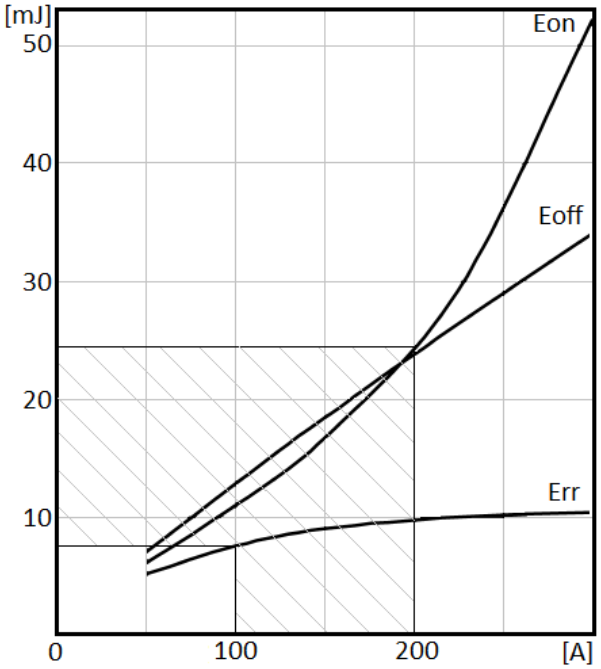

Figure 6. Accumulated energies E_{ON}, E_{off}, E_{rr}.

The temperature on the junction can be found from the dissipated power, calculated from Equation (9), thermal resistance R_{th}, and the ambient temperature T_a as follows [46–48]:

$$T_j = (P_{loss\ IGBT} \times R_{th}) + T_a, \tag{10}$$

The thermal resistance is given as:

$$P_{th} = R_{th\ j-c} + R_{th\ c-hs} + R_{th\ hs-a}, \quad (11)$$

where $R_{th\ j-c}$ is the thermal resistance junction to case; $R_{th\ c-hs}$ is the thermal resistance case to heatsink; $R_{th\ hs-a}$ is the thermal resistance heatsink to ambient.

Figure 7 shows in details the power losses and overall efficiency at the DC–DC stage of the converter during Buck mode, at switching frequency 12 kHz. The graphics are given as follows: 1–DC–DC power stage losses, dissipated from both modules M1 and M2; 2–switching and conductive losses from the IGBT transistor Q1, module M1; 3–losses from the diode D1, module M1; 4–losses from the diode D2, module M2; 5–overall efficiency of the power stage of the converter, calculated over the modules M1 and M2. As the obtained data shows, the overall efficiency does not drop under 98% at 150 A nominal current and 1000 W losses.

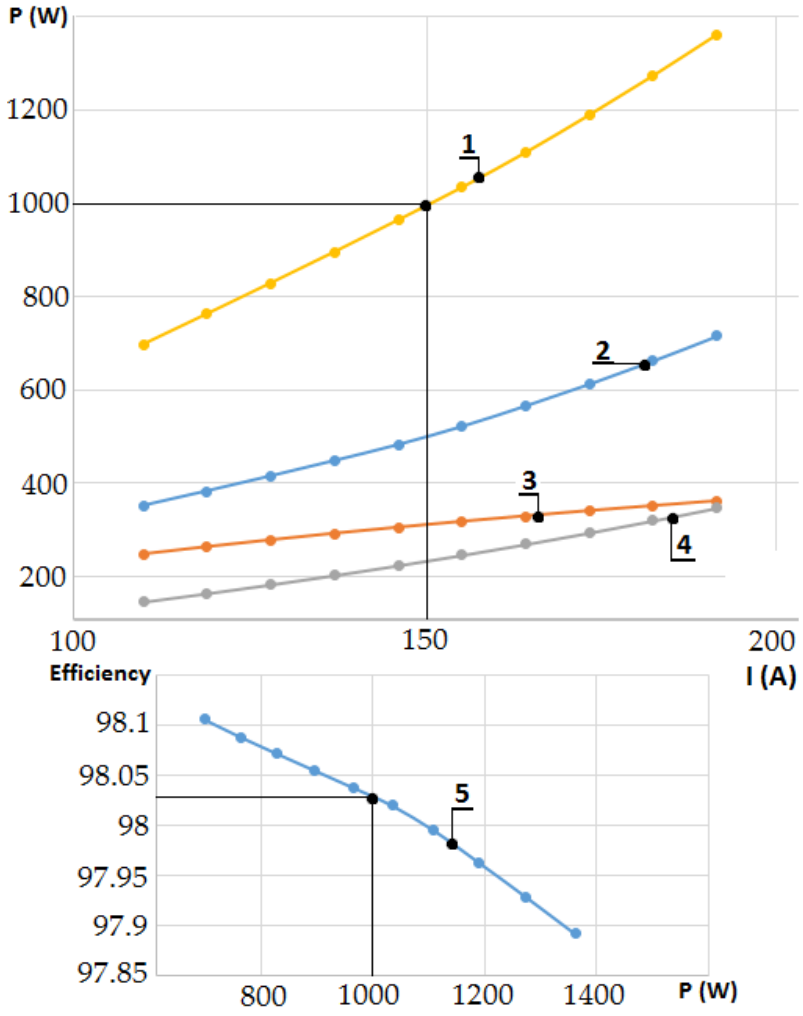

Figure 7. Buck Mode of operation. 1–DC–DC power stage losses; 2–Buck transistor Q1 losses (IGBT module M1); 3–Buck diode D1 losses (IGBT module M1); 4–Boost diode D2 losses (Boost module M2).

The same data, as a functional dependence of the duty cycle (DC), is presented in Figure 8. Graphic 1 shows linear losses increase with the DC increase, which increases the IGBT junction temperature. With a maximum junction temperature of 175 °C for silicon-based IGBTs and 15% safety margin, a temperature of 150 °C can be accepted as a maximum possible. In this analysis a constant surface temperature of 40 °C is accepted, which has to be supported by the cooling system. The data shows

that it is reached, depending on the IGBT characteristics, in the duty cycle range 0.8–0.9, which must be the maximum duty cycle for Buck mode. On the other hand, the output voltage from the Buck mode, calculated with this duty cycle range and the accepted input voltage of 660 V, gives approximately the voltage range of 550–600 V as this is suggested at the beginning in Figure 4. The results explicitly show that such frequency reduction must be applied at the end of the Buck mode, entire Buck-Boost mode and the beginning of the Boost mode.

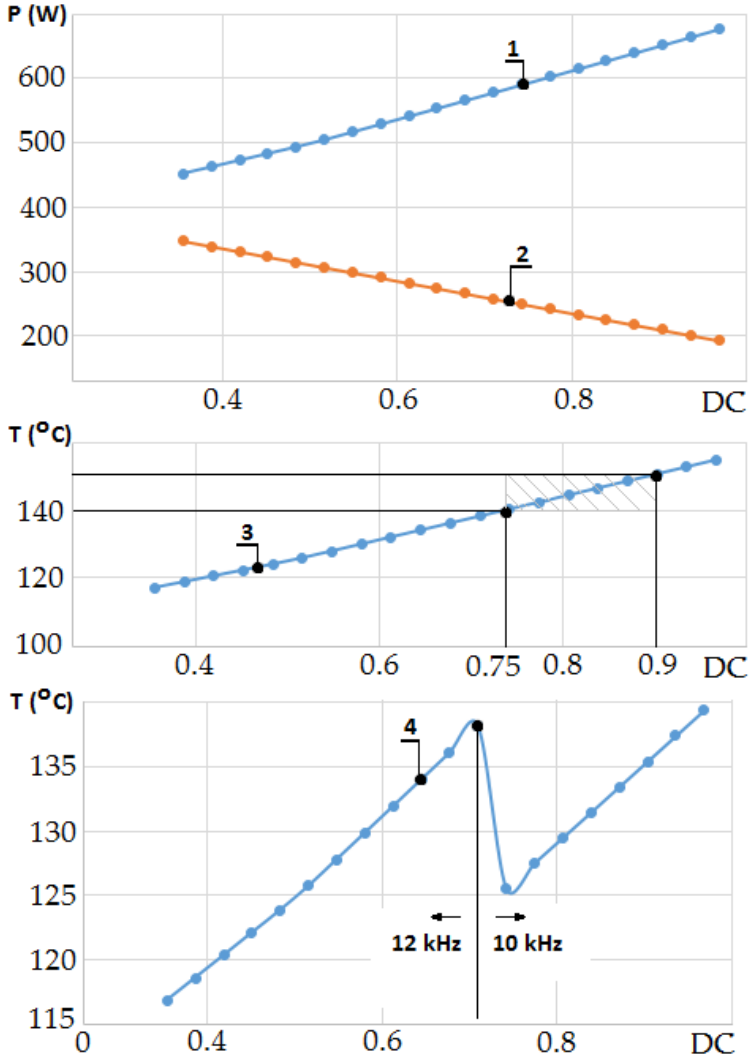

Figure 8. Buck mode of operation. 1–Buck transistor losses; 2–Buck diode losses; 3–Buck module temperature. 4–Reduction of the switching frequency from 12 kHz to 10 kHz.

The magnitude of the frequency reduction approach to decrease the junction temperature, hence losses on the power stage, is shown in Figure 8, Graphic 4. A rapid temperature drop occurs at the moment of switching frequency reduction from 12 kHz to 10 kHz. This also means that the cooling system, air or water cooled heat sink should be designed for the lower power dissipation without a need for oversizing.

Similarly, the losses for Boost operation mode are shown in Figure 9 as follows: 1–losses, dissipated from the DC–DC power stage, which includes Buck M1 and Boost M2 modules; 2–Boost transistor Q2, commutated with PWM, module M2; 3–Boost diode D2, installed in the same module; 4–conductive losses dissipated by the buck transistor, as it is permanently switched ON; 5–the efficiency is slightly slower than the expected 98%, but in the range of the acceptable error. Additionally, a comparison

between Buck (Figure 6) and Boost (Figure 8) operation modes shows that their energy characteristics are similar at the same switching frequency.

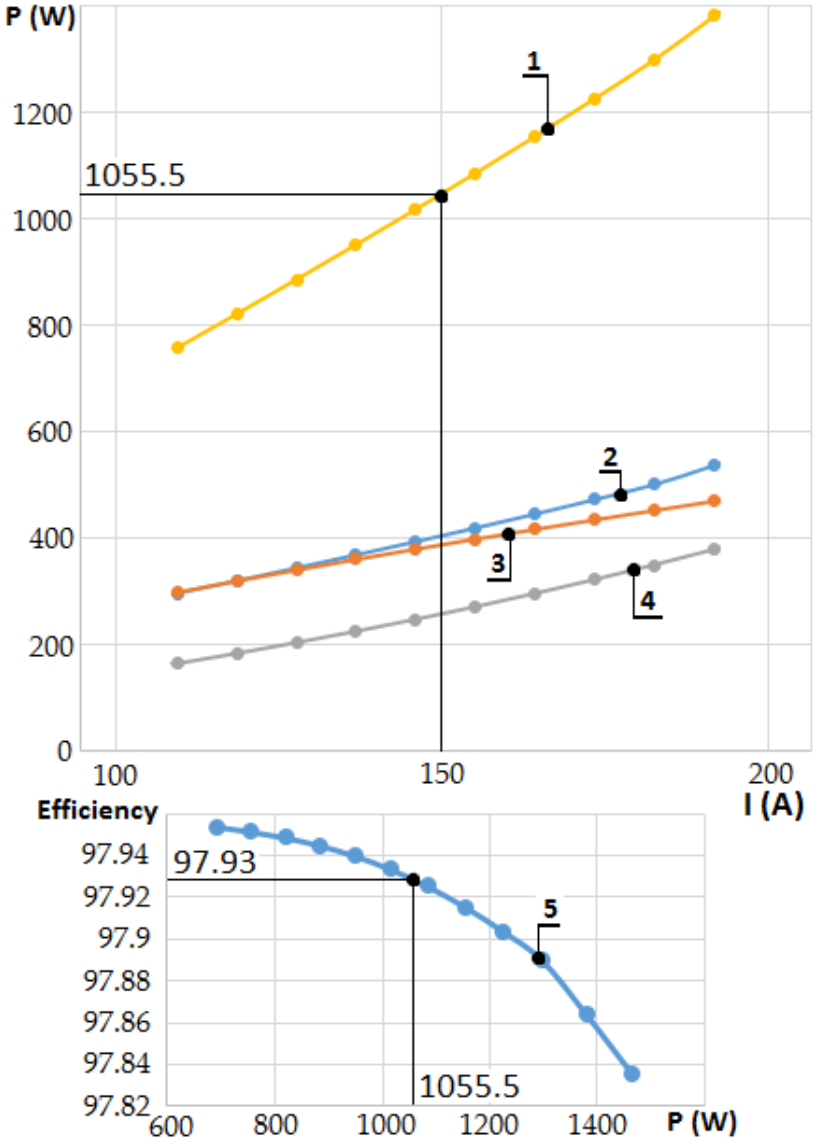

Figure 9. Boost mode of operation. 1–DC–DC power stage losses; 2–Boost transistor Q2 switching and conductive losses (IGBT module M1); 3–Boost diode D2 losses (IGBT module M1); 4–Buck transistor Q1 losses, permanently switched ON (IGBT module M2); 5–Efficiency.

Power losses at Buck-Boost operation mode are shown in Figure 10. Graphic 1 shows the dissipated losses at 12 kHz, which are approximately 300–350 W more for the entire current range than the losses at reduced to 10 kHz switching frequency (Graphic 2). Furthermore, Graphic 2 correlates with Graphic 1 (Figure 7, Buck mode) and Graphic 1 (Figure 9, Boost mode), which suggests the same losses level for the entire output voltage and current regions, shown in Figure 4.

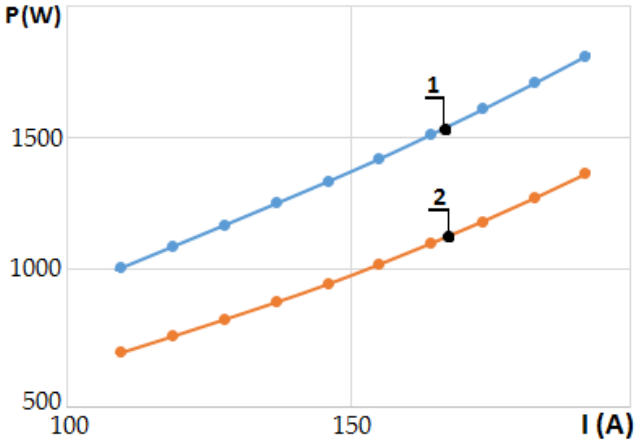

Figure 10. Buck-Boost operation mode power losses compensation with switching frequency reduction. 1–losses at 12 kHz switching frequency; 2–losses at 10 kHz switching frequency.

The output design parameters are given in Table 2. The output current ripple is calculated for the assumed output voltage range of 300–1000 V, at 150 A output nominal current, and 660 V input voltage. The inductor L1 (Figure 2) is 500 µH, which is an acceptable value for low-frequency DC–DC transformerless converters. The result shows that output voltage ripple of under 20% is achievable for the three modes of operation with the suggested frequency reduction.

Table 2. Buck-Boost converter time parameters.

Output Voltage to the Charged Battery (V)	Switching Frequency (kHz)/Period (µs)	Duty cycle	On-Time (µs)	Off-Time (µs)	Output Current Ripple (A)/(%)
Buck mode of operation (Buck module M1)					
300	12/83.33	0.45	37.93	45.41	27.31/18.2
350	12/83.33	0.53	44.23	39.1	27.42/18.28
400	12/83.33	0.61	50.54	32.79	26.28/17.52
450	12/83.33	0.68	56.85	26.49	23.88/15.92
Buck-Boost mode of operation (Buck module M1; the output voltages given for this mode of operation are after Buck module M1)					
500	10/100	0.76	75.78	24.22	24.25/16.17
525	10/100	0.79	79.57	20.43	21.48/14.32
550	10/100	0.83	83.35	16.65	18.34/12.22
Buck-Boost mode of operation (Boost module M2; the output voltages given for this mode of operation are at the output of the converter)					
600	10/100	0.17	16.76	83.24	16.76/9.3
650	10/100	0.19	19.32	80.68	20.28/10.91
700	10/100	0.22	21.51	78.49	23.66/12.38
Boost mode of operation (Boost module M2)					
750	12/83.33	0.12	10.07	73.26	13.29/7.79
800	12/83.33	0.17	14.64	68.69	19.33/10.62
850	12/83.33	0.22	18.68	64.65	24.66/12.75
900	12/83.33	0.27	22.27	61.06	29.4/14.36
950	12/83.33	0.31	25.48	57.85	33.64/15.57
1000	12/83.33	0.34	28.37	54.96	37.45/16.47

As this research is to offer more broad study, the presented data in Figures 6–9 and Table 2 are averages. It has been calculated from IGBT module datasheets, given in Table A1, using their basic parameters and the above presented equations (1–11). However, the interested reader could use

specific IGBT modules for a more precise design of a Buck-Boost converter used as a battery charger or other applications. In this case, the received results would differ from the presented data in a small acceptable range.

3. Experimental Data

The experimentally obtained oscillograms depict the most important voltages and currents waveforms for the Buck, Boost, and Buck-Boost mode of operation as follows:

Figure 11 Graphic 1 shows the drain-to-source voltage of transistor Q1, without a snubber capacitor. The experiment is conducted at nominal characteristics—switching frequency of 10–12 kHz, nominal current 150 A, output voltage within the suggested in Figure 4 range of 300–550 V, input voltage of 660 V. In this mode, the voltage peak during the switch-off period, shown in the same figure, cannot exceed the maximum rated IGBT voltage, but can make the entire system unreliable. Graphic 2 shows the current through the transistor Q1.

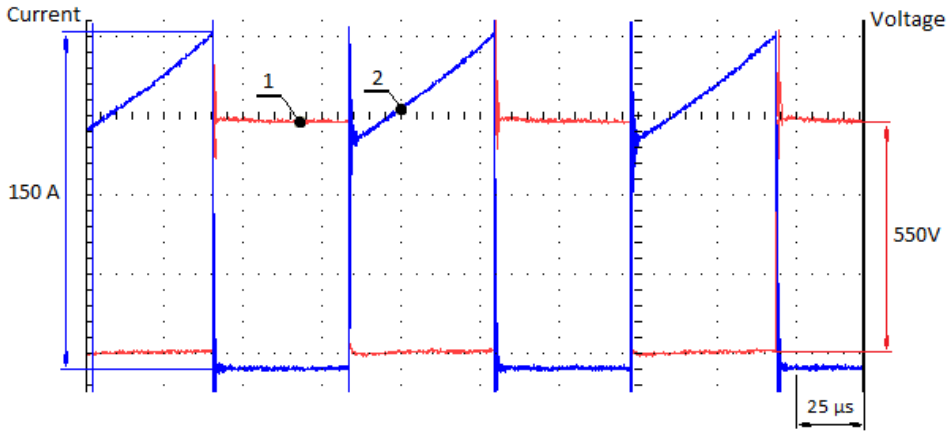

Figure 11. Buck mode of operation. 1–voltage gate-to-source Q1 (module M1, Figure 2), 2–current through transistors Q1. Snubber capacitors are not included.

Figure 12 shows the same characteristics with a snubber capacitor of 470 nF, 2 kV added in parallel to Q1. The design of this capacitor is out of the scope of this paper, but its experimental verification clearly shows its impact over the switched-off time. This oscillogram shows that the converter operates without over-voltages during the transient, but due to the capacitor included dv/dt is lower, which has negative impact on the switching losses. Hence, the converter ability to sustain the output voltage during this mode at duty cycle higher than 0.85–0.9 can be compromised.

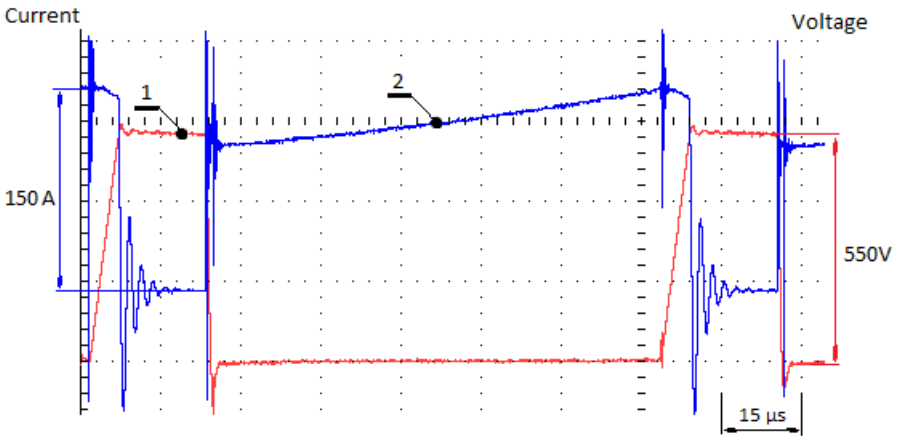

Figure 12. Buck mode of operation. 1–voltage gate-to-source Q1 (module M1), 2–current through transistors Q1. Snubber capacitors are included.

Figure 13 shows that with a duty cycle over 0.95 the IGBT module practically cannot be fully switched-off, i.e., the current is not stably established at zero ampere, which can cause unacceptable losses and overheat. This result complies with the analytical obtained result, presented above, showing that the duty cycle should be limited to 0.87–0.85 for a converter based on IGBT modules.

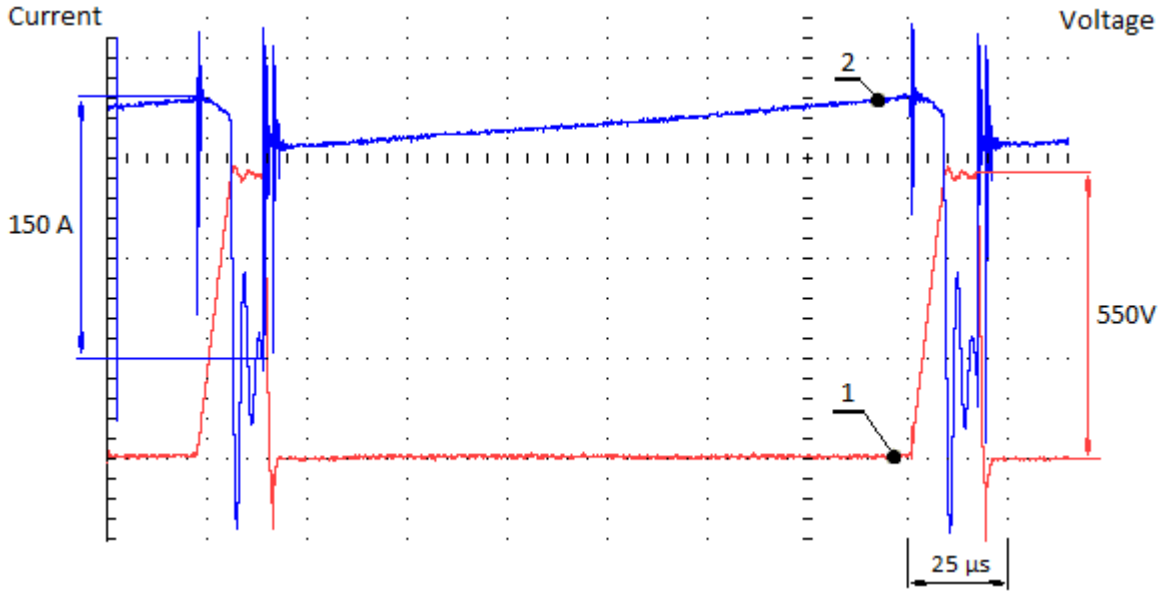

Figure 13. Buck mode of operation. 1–voltage gate-to-source Q1 (module M1), 2–current through transistors Q1. Duty cycle over 0.95.

Figure 14 the current through the inductor during the Buck mode of operation is presented. Graphic 1 shows the current through Q1 and graphic 2 the current through the diode D1, during the OFF time of the transistor Q1.

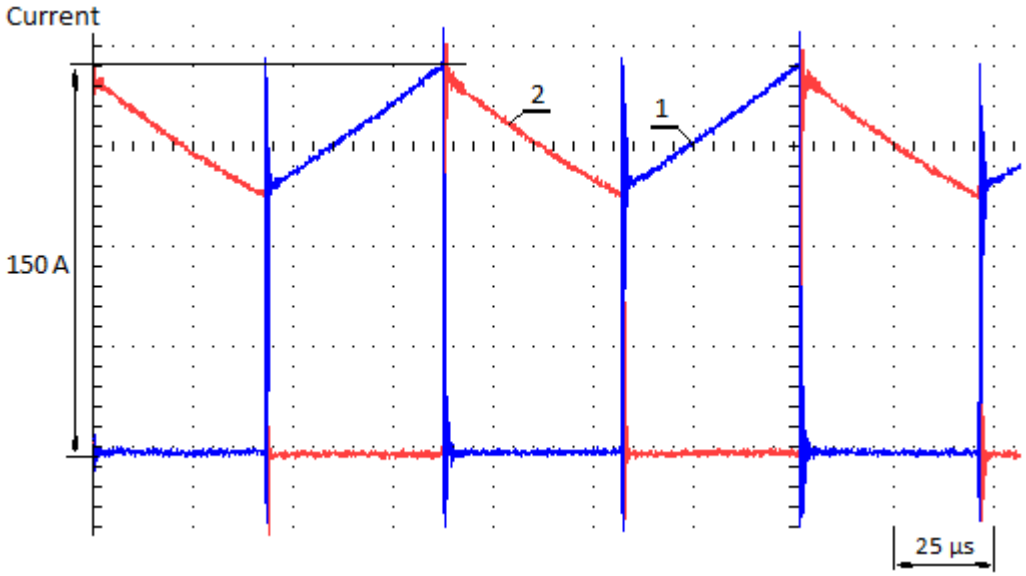

Figure 14. Buck mode of operation. Current through the inductor during 1–switched-on and 2–switched-off of transistor Q1.

Figure 15 shows the Boost mode of operation, drain-to-source voltage of the Boost transistor Q2, M2. The oscillograms in the same figure give the overvoltage of the Boost transistor and its mitigation

with the same type of snubber capacitor, connected in parallel to Q2. At the maximum accepted output voltage of 1000 V, the peak voltage can potentially exceed the rated voltage of the module of 1200 V. Having the same considerations as presented for the Buck operation mode, it can be stated that the minimum duty cycle, hence the input Boost voltage, must be limited as it is given in Figure 4.

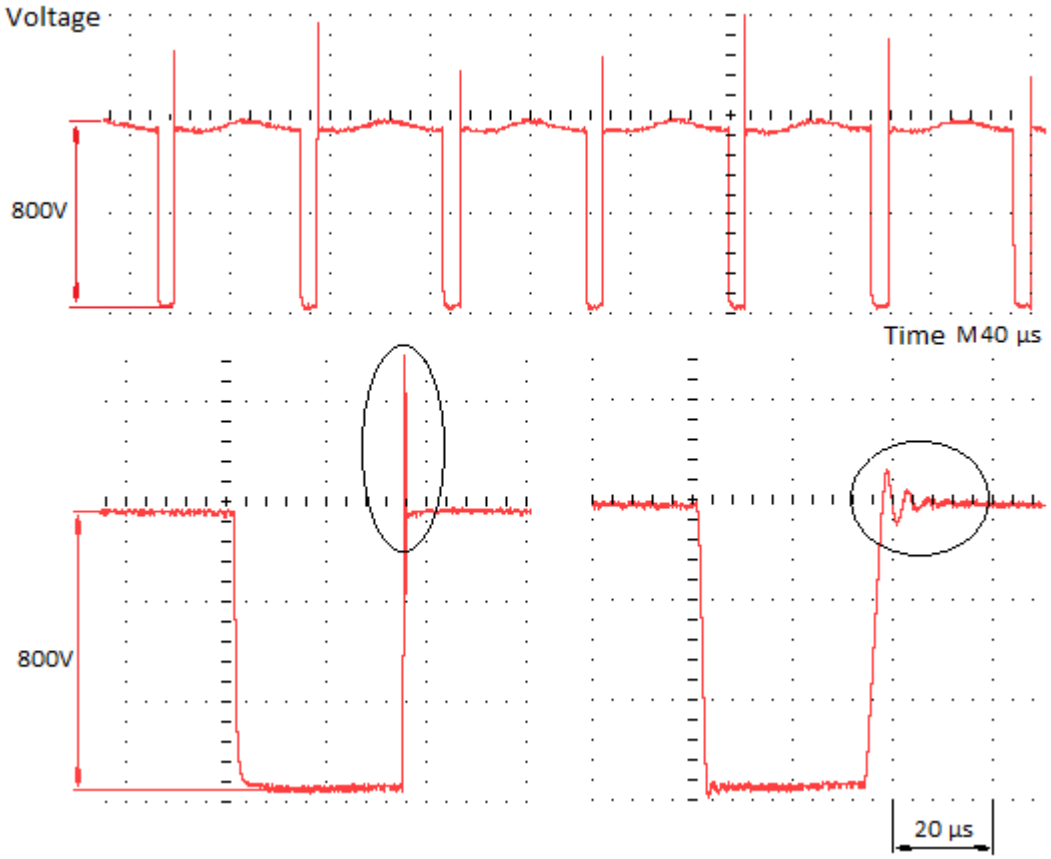

Figure 15. Boost mode of operation. Voltage drain-to-source, boost transistors Q2, module M2.

Figure 16 shows in Graphic 1 the current through the Boost transistor Q2 (switched-on) and in graphic 2-the current through the diode D2, during the switched-off period of Q2. This measurement verifies the operation of the inductor L1, Figure 2, without saturation.

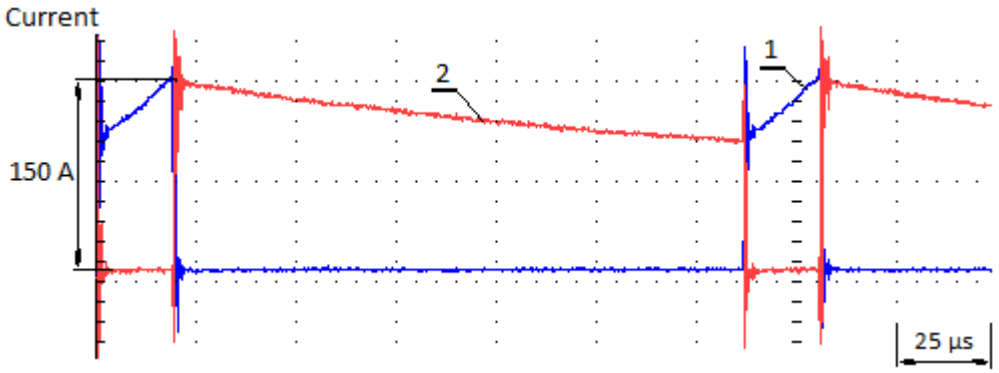

Figure 16. Boost mode of operation. 1–current through the Boost transistor Q1; 2–current through the diode D2.

Figure 17 shows the voltage (Graphic 1) and the current (Graphic 2) on the Buck side, i.e., at the input, during the Boost mode of operation is presented.

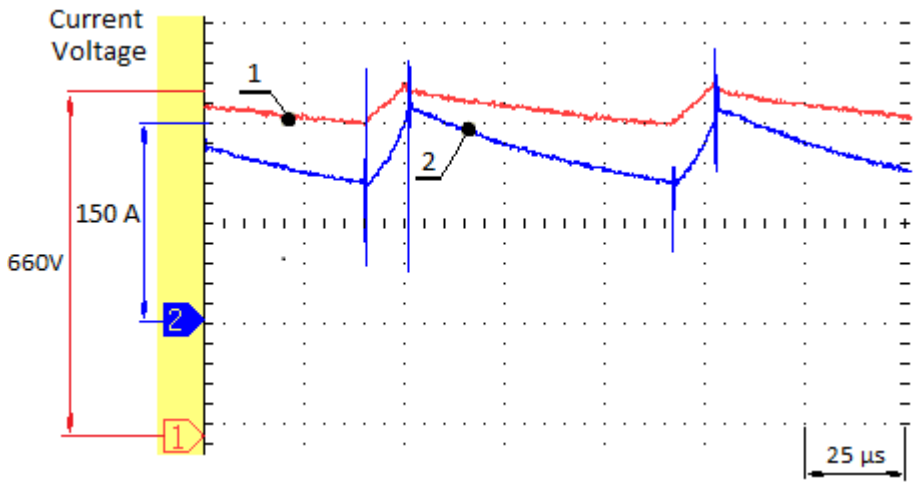

Figure 17. Boost mode of operation. 1–drain-to-source voltage, Buck transistor Q1, and 2–current through the transistor Q2 during Boost mode of operation.

Figure 18 shows that the Buck-Boost mode is depicted with the necessary PWM signals only, as all voltages and currents have similar waveforms as already presented for the previous two modes. Herein, Q1 is fixed at 0.8 PWM, Graphic 1, and Q2 is variable in the permitted range 0.1–0.4 PWM.

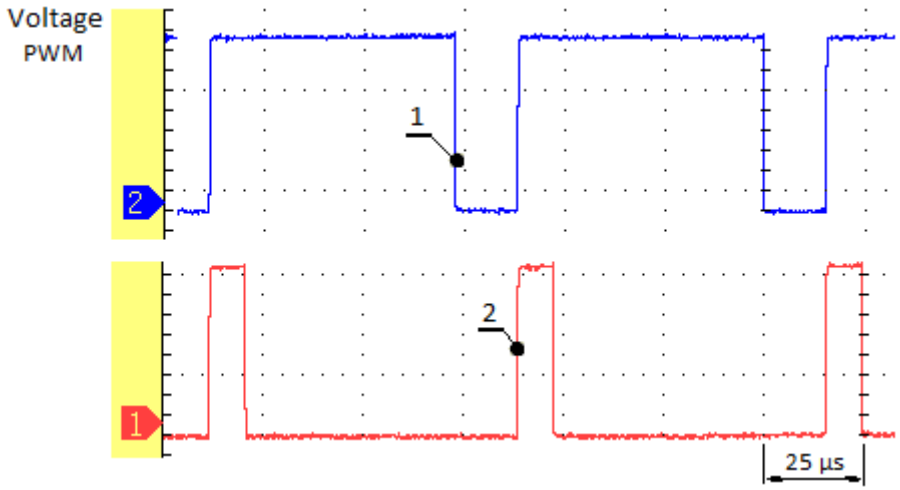

Figure 18. Buck-Boost mode of operation. 1–PWM on the Buck side, transistor Q1; 2–PWM on the Boost side, transistor Q2.

Figure 19 presents a comparison between the analytically estimated efficiency (1, 3) and experimental measurements (2, 3). This result shows that the energy analysis given in Figures 7–10 can be assumed as valid with an acceptable error under 5%.

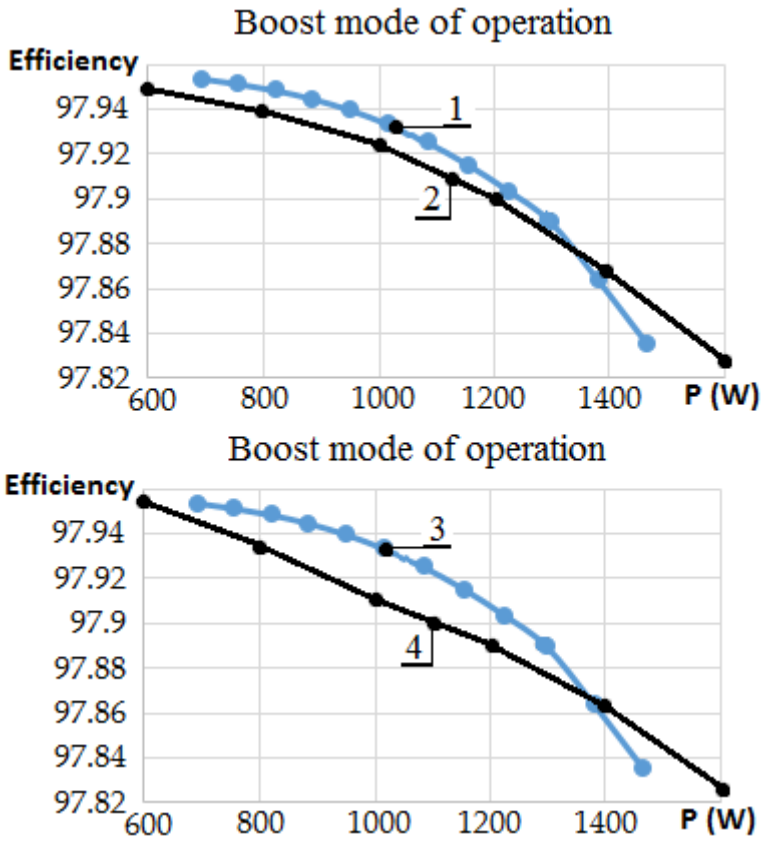

Figure 19. Comparison between analytically 1 and 3, and experimentally 2 and 4 estimated efficiency, according to Figures 7 and 9.

Figure 20 presents experimental verification of the expected temperature (2) according to the analytical calculations given in Figure 8 and experimental measurements (1). The result confirms that the concept of frequency reduction during the Buck-Boost operation mode in order the loses to be minimized and consequently temperature to be kept under the critical for the ITGT module is valid.

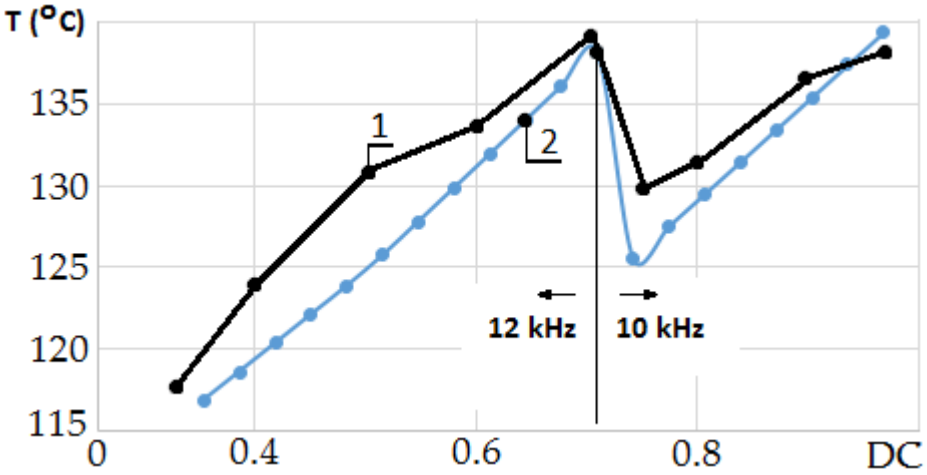

Figure 20. Comparison between analytically (2) and experimentally (1) estimated temperature, according to Figure 8.

Figure 21 shows a comparison between analytically (1, 3) and experimentally (2, 4) estimated power losses, respectively at 12 kHz switching frequency and with frequency reduction to 10 kHz. The experimentally obtained results are compared according to the analytical data from Figure 10.

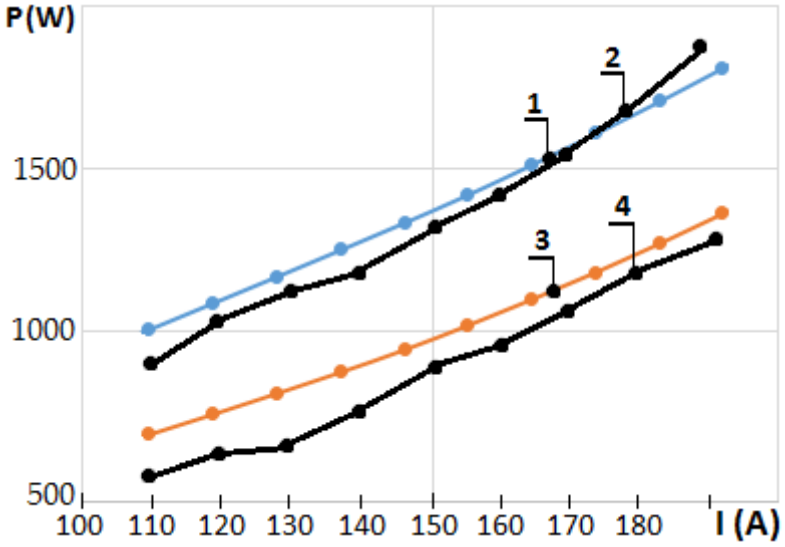

Figure 21. Comparison between analytically (1, 3) and experimentally (2, 4) estimated power losses, respectively at 12 kHz and 10 kHz, according to Figure 10.

4. Conclusions.

In this paper, a buck-boost transformer-less DC–DC converter based on high-voltage IGBT modules for use in a battery charger has been proposed, analyzed and experimentally verified.

The results explicitly showed that a Buck-Boost converter based on IGBT modules is a possible engineering solution, offering highly simple construction, high efficiency, and a wide output voltage range, which can be lower (step-down) or higher (step-up) than the input DC voltage. By adding an additional module, it can replace the commonly used Buck converter, shown in Figure 1, which operates only as a step-down converter. A converter based on IGBTs can comprise two transistor-diode modules, as Figure 2 shows, or two half-bridge modules as given in Figure 3, from the currently popular silicon-based semiconductors presented in Table A1 (applications).

The presented energy analysis showed that the converter can operate with acceptable power losses and stable thermal operation during the three modes: Buck (Figure 7), Boost (Figure 9) and Buck-Boost (Figure 10). The last requires the switching frequency to be reduced in order for equalization of the power losses, and hence the junction temperature (Figure 8, Graphic 4), to be achieved for the entire voltage range suggested in Figure 4. It has been found that the suitable switching frequency for this class of hard-switched converters, considering the required power and IGBT parameters, is around 12 kHz, reduced to 10 kHz in the Buck-Boost operation mode.

The experimental data, presented in Figures 11–21, show that the presented concept can be realized with IGBT modules comprised of transistor-diode structures at the required power. The converter operates stably for the entire range of switching frequencies, which is depicted with oscillograms in Figures 11–17. The suggested control conception according to which the switching frequency must be reduced during Buck-Boost mode of operation in order for the temperature to be kept under the maximum junction temperature with a safety merging is verified experimentally, Figures 19–21.

Although the presented research is limited to the power part of the suggested converter, the analysis and experimental verification show that a powerful Buck-Boost converter for battery charging, based on a minimum number of modules, is a possible solution. A flexible frequency switching control has the magnitude to guarantee a thermal equilibrium of the IGBT modules without power reduction during the entire Buck, Boost and Buck-Boost modes.

Author Contributions: B.D. conceived the idea. B.D., K.H., S.B. and G.C. made substantial contributions to conception, design, analysis and experimental verification. S.S. and A.C. contributed to the final edition. All authors have jointly and equally approved the final version. All authors have read and agreed to the published version of the manuscript.

Funding: This research received no external funding.

Acknowledgments: The authors would like to thank the company Bowman Power, Southampton, UK, for their kind support during the development of this research.

Conflicts of Interest: The authors declare no conflict of interest.

Appendix A

Table A1. IGBT modules, suitable for the proposed converter.

Type	Voltage [V]	Current [A]	E_{on} [mJ]	E_{off} [mJ]	E_r [mJ]	$R_{th(j-c)}$ [K/W]
Semikron [49]						
SEMiX452GAL126HDs	1200	319	35	45	33	0.15
SKM400GB125D		300	17	18	16	0.05
SKM400GAL126D SKM400GAR126D		300	29	48	27	0.08
SEMiX302GAL12E4s SEMiX302GAR12E4s		356	30	44	19	0.096
SKiiP39GB12E4V1		312	20	49.7	30.2	0.19
SEMiX503GB126HDs		466	20	44	32.5	0.08
Infineon [50]						
FF300R12KS4HOSA1	1200	300	25	15	15	0.064
FF300R12KE3HOSA1		440	25	44	26	0.15
FF450R12KT4		450	30	40	35	0.11
Mitsubishielectric [51]						
CM300DX-24T1	1200	300	36	29	18	0.1
CM450DX-24T1		450	56.6	42	23	0.08
Fuji electric [52]						
2MBI300U4H-120	1200	300	17	19	10	0.08
2MBI400VD-120-50		400	16	18	17	0.045
1MBI200VA-120L-50		200	15	22	18	0.17
1MBI900VXA-120PC-50 1MBI900VXA-120PD-50		900	20	40	15	0.03
Microsemi [53]						
APTGT200A120G	1200	400	20	20	18	0.14
IXYS [54]						
MIXA225PF1200TSF	1200	360	20	27	11.7	0.14
MID 300-12A4 MDI 300-12A4		330	32	29	-	0.15
MID 550-12 A4 MDI 550-12 A4		460	64	59	-	0.05

References

1. Wolbertus, R.; Hoed, R.V.D. Electric Vehicle Fast Charging Needs in Cities and along Corridors. *World Electr. Veh. J.* **2019**, *10*, 45. [CrossRef]
2. Khan, W.; Ahmad, F.; Alam, M.S. Fast EV charging station integration with grid ensuring optimal and quality power exchange. *Eng. Sci. Technol. Int. J.* **2019**, *22*, 143–152. [CrossRef]
3. Neaimeha, M.; Salisbury, S.; Hill, G.; Blythe, P.; Scoffield, D.; Francfort, J. Analysing the usage and evidencing the importance of fast chargers for the adoption of battery electric vehicles. *Energy Policy* **2017**, *108*, 474–486. [CrossRef]
4. Gnanna, T.; Funkea, S.; Jakobsson, N.; Plotza, P.; Sprei, F.; Bennehag, A. Fast charging infrastructure for electric vehicles: Today's situation and future needs. *Transp. Res. Part. D Transp. Environ.* **2018**, *62*, 314–329. [CrossRef]
5. Kim, D.H.; Kim, M.S.; Nengroo, S.H.; Kim, C.H.; Kim, H.J. LLC Resonant Converter for LEV (Light Electric Vehicle) Fast Chargers. *Electronics* **2019**, *8*, 362. [CrossRef]

6. Yan, X.; Li, J.; Zhang, B.; Jia, Z.; Tian, Y.; Zeng, H.; Lv, Z. Virtual Synchronous Motor Based-Control of a Three-Phase Electric Vehicle Off-Board Charger for Providing Fast-Charging Service. *Appl. Sci.* **2018**, *8*, 856. [CrossRef]
7. Lia, J.; Wang, D.; Wang, W.; Jiang, J. Minimize Current Stress of Dual-Active-Bridge DC-DC Converters for Electric Vehicles Based on Lagrange Multipliers Method. *Energy Procedia* **2017**, *105*, 2733–2738. [CrossRef]
8. Lee, I.; Lee, J. A High-Power DC-DC Converter Topology for Battery Charging Applications. *Energies* **2017**, *10*, 871. [CrossRef]
9. Al-Ogaili, A.; Aris, I.; Verayiah, R.; Ramasamy, A.; Marsadek, M.; Rahmat, N.; Hoon, Y.; Aljanad, A.; Al-Masri, A. A Three-Level Universal Electric Vehicle Charger Based on Voltage-Oriented Control and Pulse-Width Modulation. *Energies* **2019**, *12*, 2375. [CrossRef]
10. Khan, S.; Mehmood, K.; Haider, Z.; Bukhari, S.; Lee, S.; Rafique, M.; Kim, C. Energy Management Scheme for an EV Smart Charger V2G/G2V Application with an EV Power Allocation Technique and Voltage Regulation. *Appl. Sci.* **2018**, *8*, 648. [CrossRef]
11. Perpina, X.; Serviere, J.F.; Jorda, X.; Fauquet, A.; Hidalgo, S.; Ibanez, J.; Rebollo, J.; Mermet-Guyennet, M. IGBT module failure analysis in railway applications. *Microelectron. Reliab.* **2008**, *48*, 1427–1431. [CrossRef]
12. Gorecki, P.; Gorecki, K. Modelling a Switching Process of IGBTs with Influence of Temperature Taken into Account. *Energies* **2019**, *12*, 1894. [CrossRef]
13. Napoli, F.; Magnani, A.; Coppola, M.; Guerriero, P.; D'Alessandro, V.; Codecasa, L.; Tricoli, P.; Daliento, S. On-Line Junction Temperature Monitoring of Switching Devices with Dynamic Compact Thermal Models Extracted with Model Order Reduction. *Energies* **2017**, *10*, 189. [CrossRef]
14. Chang, Y.; Li, W.; Luo, H.; He, X.; Iannuzzo, F.; Blaabjerg, F.; Lin, W. A 3D Thermal Network Model for Monitoring Imbalanced Thermal Distribution of Press-Pack IGBT Modules in MMC-HVDC Applications. *Energies* **2019**, *12*, 1319. [CrossRef]
15. Lucas, A.; Trentadue, G.; Scholz, H.; Otura, M. Power Quality Performance of Fast-Charging under Extreme Temperature Conditions. *Energies* **2018**, *11*, 2635. [CrossRef]
16. Hocine, R.; Pulko, S.; Stambouli, A.; Saidane, A. TLM method for thermal investigation of IGBT modules in PWM mode. *Microelectron. Eng.* **2009**, *86*, 2053–2062. [CrossRef]
17. An, N.; Du, M.; Hu, Z.; Wei, K. A High-Precision Adaptive Thermal Network Model for Monitoring of Temperature Variations in Insulated Gate Bipolar Transistor (IGBT) Modules. *Energies* **2018**, *11*, 595. [CrossRef]
18. Jung, E.; Cho, Y.; Kang, E.; Kim, Y.; Sung, M. A Study on the Design and Electrical Characteristics Enhancement of the Floating Island IGBT with Low On-Resistance. *J. Electr. Eng. Technol.* **2012**, *7*, 601–605. [CrossRef]
19. Huang, X.; Chang, D.; Ling, C.; Zheng, T. Research on Single-Phase PWM Converter with Reverse Conducting IGBT Based on Loss Threshold Desaturation Control. *Energies* **2017**, *10*, 1845. [CrossRef]
20. Huang, X.; Ling, C.; Chang, D.; You, X.; Zheng, T. Loss Characteristics of 6.5 kV RC-IGBT Applied to a Traction Converter. *Energies* **2017**, *10*, 891. [CrossRef]
21. Benmansour, A.; Azzopardi, S.; Martin, J.; Woirgard, E. Trench IGBT failure mechanisms evolution with temperature and gate resistance under various short-circuit conditions. *Microelectron. Reliab.* **2007**, *47*, 1730–1734. [CrossRef]
22. Benmansour, A.; Azzopardi, S.; Martin, J.C.; Woirgard, E. A step by step methodology to analyze the IGBT failure mechanisms under short circuit and turn-off inductive conditions using 2D physically based device simulation. *Microelectron. Reliab.* **2007**, *47*, 1800–1805. [CrossRef]
23. Jeong, J.; Hong, S.; Park, S. Field failure mechanism and improvement of EOS failure of integrated IGBT inverter modules. *Microelectron. Reliab.* **2007**, *47*, 1795–1799. [CrossRef]
24. Belmehdi, Y.; Azzopardi, S.; Benmansour, A.; Deletage, J.; Woirgard, E. Uni-axial mechanical stress effect on Trench Punch through IGBT under short-circuit operation. *Microelectron. Reliab.* **2009**, *49*, 1398–1403. [CrossRef]
25. Urresti-Ibanez, J.; Castellazzi, A.; Piton, M.; Rebollo, J.; Mermet-Guyennet, M.; Ciappa, M. Robustness test and failure analysis of IGBT modules during turn-off. *Microelectron. Reliab.* **2007**, *47*, 1725–1729. [CrossRef]
26. Busatto, G.; Abbate, C.; Abbate, B.; Iannuzzo, F. IGBT modules robustness during turn-off commutation. *Microelectron. Reliab.* **2008**, *48*, 1435–1439. [CrossRef]

27. Chen, L.; Xu, J.; Cheng, S.; Liu, L.; Deng, L. Stability analysis and AC modeling of high-efficiency Buck/Boost converter. In Proceedings of the 2008 IEEE International Conference on Electron Devices and Solid-State Circuits, Hong Kong, China, 8–10 December 2008.
28. Ren, X.; Ruan, X.; Qian, H.; Li, M.; Chen, Q. Dual-Edge Modulated Four-Switch Buck-Boost Converter. In Proceedings of the IEEE Power Electronics Specialists Conference, Rhodes, Greece, 15–19 June 2008.
29. Wei, C.; Chen, C.; Wu, K.; Ko, I. Design of an Average-Current-Mode Noninverting Buck–Boost DC–DC Converter with Reduced Switching and Conduction Losses. *IEEE Trans. Power Electron.* **2012**, *27*, 1894. [CrossRef]
30. Lin, R.; Wang, R. Non-inverting Buck-Boost Power-Factor-Correction Converter with Wide Input-Voltage-Range Applications. In Proceedings of the 36th Annual Conference on IEEE Industrial Electronics Society, Glendale, AZ, USA, 7–10 November 2010.
31. Zhang, F.; Xu, J.; Yang, P.; Chen, Z. Single-Phase Two-Switch PCCM Buck-Boost PFC Converter with Fast Dynamic Response for Universal Input Voltage. In Proceedings of the 8th International Conference on Power Electronics—ECCE Asia, The Shilla Jeju, Korea, 30 May–3 June 2011.
32. Ren, X.; Tang, Z.; Ruan, X.; Wei, J.; Hua, G. Four Switch Buck-Boost Converter for Telecom DC-DC Power Supply Applications. In Proceedings of the Twenty-Third Annual IEEE Applied Power Electronics Conference and Exposition, Austin, TX, USA, 24–28 February 2008.
33. Dening, D. A buck-or-boost converter module with embedded inductor and fast current limit. *IEEE Trans. Power Electron.* **2011**, *26*, 3874–3883. [CrossRef]
34. Shiau, J.; Cheng, C. Design of a non-inverting synchronous Buck-Boost DC/DC power converter with moderate power level. *Robot. Comput. Manuf.* **2010**, *26*, 263–267. [CrossRef]
35. Angkititrakul, S.; Hu, H.; Liang, Z. Active Inductor Current Balancing for Interleaving Multi-Phase Buck-Boost Converter. In Proceedings of the Twenty-Fourth Annual IEEE Applied Power Electronics Conference and Exposition, Washington, DC, USA, 15–19 February 2009.
36. Chang, C.; Wei, C. Single-inductor four-switch non-inverting buck-boost dc-dc converter. In Proceedings of the 2011 International Symposium on VLSI Design, Automation and Test, Hsinchu, Taiwan, 25–28 April 2011.
37. Lee, Y.; Khaligh, A.; Chakraborty, A.; Emadi, A. Digital Combination of Buck and Boost Converters to Control a Positive Buck–Boost Converter and Improve the Output Transients. *IEEE Trans. Power Electron.* **2009**, *24*, 1267–1279. [CrossRef]
38. Application note AN4449, Buck-Boost Converter Using the STM32F334 Discovery kit, STMicroelectronics. 2014. Available online: https://www.st.com/resource/en/application_note/dm00108726.pdf (accessed on 27 February 2020).
39. Application note TND6253/D, Dv/dt Induced False Turn−on Issue in 4-Switch Noninverting Buck-Boost Converters, Semiconductor Components Industries, LLC. September 2018. Available online: https://www.onsemi.com/pub/Collateral/TND6253-D.PDF (accessed on 27 February 2020).
40. Application Note SLVA535A, Basic Calculations for Buck-Boost Converters, Texas Instruments 2012. Available online: www.ti.com/lit/an/slva535b/slva535b.pdf (accessed on 27 February 2020).
41. Application Note: PMP21529, 4-Switch Buck-Boost Bi-Directional DC-DC Converter Reference Design. Available online: www.ti.com/lit/ug/tidt046/tidt046.pdf (accessed on 27 February 2020).
42. Pressman, A. *Switching Power Supply Design*; McGraw-Hill, Inc.: New York, NY, USA, 1998.
43. Billings, K.; Morey, T. *Switch Mode Power Supply Handbook*, 3rd ed. 2011. Available online: https://lib.hpu.edu.vn/handle/123456789/23388 (accessed on 27 February 2020).
44. IGBT Application Note, R07AN0001EJ0410, Renesas Electronics, Rev.4.10. Available online: https://www.renesas.com/us/en/doc/products/igbt/apn/r07an0001ej0410_igbt.pdf (accessed on 27 February 2020).
45. Wintrich, A.; Nicolai, U.; Tursky, W.; Reimann, T. Application Manual Power Semiconductors, SEMIKRON International 2015. Available online: https://www.semikron.com/dl/service-support/downloads/download/semikron-application-manual-power-semiconductors-english-en-2015.pdf (accessed on 27 February 2020).
46. Baliga, B. The IGBT Device Physics, Design and Applications of the Insulated Gate Bipolar Transistor. Elsevier Inc., 2015. Available online: https://www.elsevier.com/books/the-igbt-device/baliga/978-1-4557-3143-5 (accessed on 27 February 2020).
47. Volke, A.; Hornkamp, M. *IGBT Modules, Technology, Driver and Application*; Infineon Technologies AG: Neubiberg, Germany, 2017.

48. Khanna, V. *The Insulated Gate Bipolar Transistor IGBT Theory and Design*; Wiley-Interscience: Piscataway, NJ, USA, 2003; ISBN 0-471-23845-7.
49. IGBT Generation 7. The New Benchmark for Motor Drives. Available online: https://www.semikron.com/ (accessed on 27 February 2020).
50. Infineon Technologies: Semiconductor & System Solutions. Available online: https://www.infineon.com/ (accessed on 27 February 2020).
51. Mitsubishi Electric Global Website. Available online: http://www.mitsubishielectric.com/ (accessed on 27 February 2020).
52. Fuji Electric Global. Available online: https://www.fujielectric.com/ (accessed on 27 February 2020).
53. Microsemi: Semiconductor & System Solutions, Power Matters. Available online: https://www.microsemi.com/ (accessed on 27 February 2020).
54. Littelfuse Coompletes IXYS Acquisition. Available online: http://www.ixys.com/ (accessed on 27 February 2020).